Excitonic effects in the optical spectrum of GaAs

Sadao Adachi
Department of Electronic Engineering, Faculty of Engineering, Gunma University, Kiryu-shi, Gunma 376, Japan
(Received 5 May 1989; revised manuscript received 1 August 1989)

We present a calculation of the real (ϵ_1) and imaginary (ϵ_2) parts of the dielectric function of semiconductors at energies below and above the fundamental absorption edge. This model includes the E_0, $E_0+\Delta_0$, E_1, $E_1+\Delta_1$, and $E_2(E_0')$ gaps as the main dispersion mechanisms. The model is also made to account for the excitonic effects at these critical points (CP's). A model analysis indicates that the inclusion of the excitonic effects in our one-electron model corrects the strength of the peaks in the correct direction with experimental information (i.e., the E_1 peak becomes stronger and the E_2 peak weaker). Detailed analyses are presented for GaAs in the temperature range between 22–754 K, and results are in satisfactory agreement with the experimental data over the entire range of photon energies (0.0–6.0 eV). The temperature dependence of the strength and the broadening parameters at each CP are also given and discussed.

I. INTRODUCTION

GaAs is a material of great physical interest and technological importance for many high-speed electronic and optoelectronic devices. Investigation of the dielectric behaviors in solids is an old topic which arises in strong connection with the fundamental optical properties of the solids.[1] Knowledge of the refractive indices and absorption coefficients of semiconductors is especially important in the design of heterostructure lasers as well as other waveguiding devices using these materials.[2] The dielectric function, $\epsilon(\omega)=\epsilon_1(\omega)+i\epsilon_2(\omega)$, can describe such an optical response of the medium at all photon energies $E=\hbar\omega$.[1]

Spectroscopic ellipsometry is known to be highly suitable for determining the dielectric function of semiconductors.[3] Recently, Lautenschlager *et al.*[4] have studied the temperature dependence of the dielectric function of GaAs in the temperature range between 20 and 754 K by spectroscopic ellipsometry ($E=1.3$–5.5 eV). The structures observed in the $\epsilon(\omega)$ spectra were attributed to interband critical points (CP's), which can be analyzed in terms of standard analytical line shapes:

$$\epsilon(\omega)=C^*-A^*e^{i\phi}(\hbar\omega-E_c+i\Gamma)^n .$$

They determined the CP parameters' amplitude A^*, energy threshold E_c, broadening Γ, and excitonic phase angle ϕ for each CP [E_0, $E_0+\Delta_0$, E_1, $E_1+\Delta_1$, and E_2 (E_0')]. However, unfortunately, this expression is not suitable for describing the dielectric behavior $\epsilon(\omega)$ over the entire range of photon energies.

In our preceding papers,[5–11] we demonstrated a method for calculation of the dielectric function $\epsilon(\omega)$ of the diamond-type (Si, Ge, and α-Sn) and zinc-blende-type semiconductors (GaP, InAs, $Al_xGa_{1-x}As$, $In_{1-x}Ga_xAs_yP_{1-y}$, etc.). Excellent agreement has been achieved between our model and experimental information over the entire range of photon energies ($E=0.0$–6.0 eV). However, in these analyses we have paid no attention to the excitonic effects of the optical spectra for these semiconductors. This is because our analyzed data were obtained at moderately high temperature (i.e., room temperature). At low temperatures, optical spectra may not be explained within the framework of the one-electron approximation we used, since the excitonic effect may profoundly modify the CP singularity structure at low temperatures.

There are many theoretical works[12–20] dealing with the excitonic effects on optical spectra of semiconductors. Some theoretical evaluations[15,19,20] showed that the excitonic effects account for the discrepancies in the ϵ_2 strengths of the E_1 and E_2 peaks in semiconductors: The inclusion of the excitonic effects in the one-electron band model corrects the strength of the peaks in the correct direction with the experimental information (i.e., it leads to strengthening of the E_1 peak and weakening of the E_2 peak). However, these theories have one disadvantage in the sense that they are not expressed as continuous analytical functions of the CP parameters and photon energies.

In this paper we present a method for calculation of the spectral dependence of the dielectric function $\epsilon(\omega)$ of GaAs. The model is based on the Kramers-Kronig (KK) transformation and is strongly connected with the electronic energy-band structures of the medium. The model covers the optical response of semiconductors over the entire range of photon energies at various temperatures. In Sec. II we describe the details of our model, which includes the E_0, $E_0+\Delta_0$, E_1, $E_1+\Delta_1$, and E_2 (E_0') gaps as the main dispersion mechanisms. A model is also made to account for the excitonic effects at these CP's. In Sec. III we show the fits with our model to the experimental data of GaAs reported by Lautenschlager *et al.* (Ref. 4) and Aspnes and Studna (Ref. 3). The temperature dependence of the strength and the broadening parameters at each CP are also presented and discussed in Sec. III. Finally, in Sec. IV the conclusions obtained in this study are summarized briefly.

II. THEORETICAL MODEL

A. E_1 and $E_1+\Delta_1$ transitions

The E_1 and $E_1+\Delta_1$ transitions in GaAs may take place along the $\langle 111 \rangle$ directions (Λ) or at L points in the Brillouin zone (BZ). These transitions are of the three-dimensional (3D) M_1 type. The contributions to ϵ_2 of this type of noninteracting electron-hole pairs are given by (Refs. 5–9)

$$\epsilon_2(\omega)=\begin{cases}\pi\chi_1^{-2}[B_1-B_{11}(E_1-\hbar\omega)^{0.5}] & (\hbar\omega<E_1),\\ \pi B_1\chi_1^{-2} & (\hbar\omega\geq E_1),\end{cases} \tag{1a}$$

for the E_1 transitions, and

$$\epsilon_2(\omega)=\begin{cases}\pi\chi_{1s}^{-2}[B_2-B_{21}(E_1+\Delta_1-\hbar\omega)^{0.5}]\\ (\hbar\omega<E_1+\Delta_1),\\ \pi B_2\chi_{1s}^{-2} & (\hbar\omega\geq E_1+\Delta_1),\end{cases} \tag{1b}$$

for the $E_1+\Delta_1$ transitions, where

$$\chi_1=\hbar\omega/E_1 , \tag{2}$$

$$\chi_{1s}=\hbar\omega/(E_1+\Delta_1) . \tag{3}$$

In Eq. (1), the B's are the strength parameters of the noninteracting electron-hole excitations at the 3D M_1 CP's.

Since the M_1 CP longitudinal effective mass m_L is much larger than its transverse counterparts, the m_T's, one can treat these 3D M_1 CP's as two-dimensional minima M_0. The contribution to ϵ_2 of this type of 2D minimum is given by

$$\epsilon_2(\omega)=\pi[B_1\chi_1^{-2}H(\chi_1-1)+B_2\chi_{1s}^{-2}H(\chi_{1s}-1)] , \tag{4}$$

where

$$H(z)=\begin{cases}1 & \text{for } z\geq 0,\\ 0 & \text{for } z<0.\end{cases} \tag{5}$$

We have already shown[5–11] that a calculation of Eq. (1) or (4) satisfactorily interprets experimental ϵ_2 spectra (taken at room temperature) of various semiconductors in these transition regions. However, it is worth noting that the model of Eq. (1) or (4) does not account for any thermal-broadening effect. It is well known that the optical transitions are strongly affected by a thermal-broadening effect, i.e., a lifetime broadening. We now thus present a new expression for ϵ_2 of the $E_1/(E_1+\Delta_1)$ transitions:

$$\epsilon_2(\omega)=\chi_1^{-2}\{B_{01}^{*}-\mathrm{Im}[B_1\ln(\hbar\omega-E_1+i\Gamma)]\}+\chi_{1s}^{-2}\{B_{02}^{*}-\mathrm{Im}[B_2\ln(\hbar\omega-E_1-\Delta_1+i\Gamma)]\} , \tag{6}$$

where B_{01}^{*} and B_{02}^{*} are the constants and Γ is the broadening (damping) energy. The first and second terms on the right-hand side of Eq. (6), respectively, correspond to the E_1 and $E_1+\Delta_1$ gap contributions. The dependence of ϵ_2 on frequency ω obtained from this expression is shown in Fig. 1. The numerical values used in the calculations correspond to those for GaAs at 22 K (see Table I). The theoretical ϵ_2 spectrum with $\Gamma=0$ eV shows a sharp cutoff end at the low-energy side of E_1. This spectrum exactly agrees with that of Eq. (4) (2D M_0 CP's). A consideration of the broadening effect decreases the ϵ_2 value with shifting of its peak energy toward the higher-energy side. The spectrum can then be characterized by a steep low-energy side and a broader high-energy side: it bears a strong resemblance to the spectrum of Eq. (1) (3D M_1 CP's).

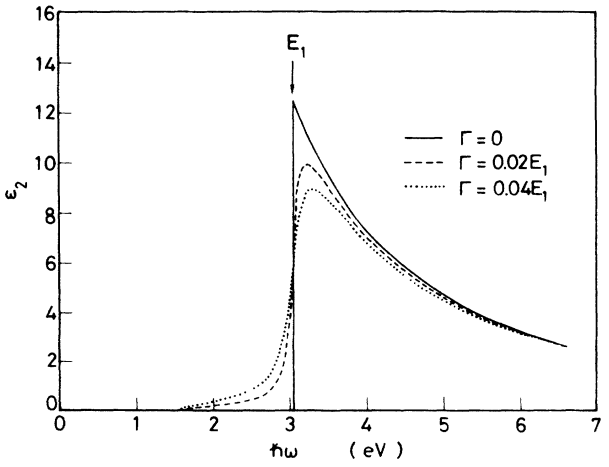

FIG. 1. Line shape of the E_1 gap contribution to $\epsilon_2(\omega)$ for GaAs [Eq. (6)] with three different broadening parameters ($\Gamma=0$, $0.02E_1$, and $0.04E_1$).

The KK transformation of Eq. (4) [Eq. (6)] gives

$$\epsilon_1(\omega)=\mathrm{Re}\epsilon(\omega)$$
$$=\mathrm{Re}[-B_1\chi_{1d}^{-2}\ln(1-\chi_{1d}^{2})-B_2\chi_{1sd}^{-2}\ln(1-\chi_{1sd}^{2})] , \tag{7}$$

where

$$\chi_{1d}=(\hbar\omega+i\Gamma)/E_1 , \tag{8}$$

$$\chi_{1sd}=(\hbar\omega+i\Gamma)/(E_1+\Delta_1) . \tag{9}$$

As mentioned in our previous papers,[5–9] expression (7) with $\Gamma=0$ eV exhibits a divergence at the E_1 and $E_1+\Delta_1$ CP's. The broadening effect can successfully decrease the ϵ_1 strength of the $E_1/(E_1+\Delta_1)$ structure and lead to a fact which is coincident with experimental verification.

Excitonic states should, in principle, exist at each type of CP, since the Coulomb-like interaction is always

TABLE I. Parameters used in the calculations of $\epsilon_2(\omega)$ and $\epsilon_1(\omega)$.

Parameter	Temperature (K) 22	253	300	504	754
E_0 (eV)	1.52	1.44	1.42	1.33	1.20
$E_0+\Delta_0$ (eV)	1.85	1.78	1.75	1.66	1.54
E_1 (eV)	3.04	2.94	2.91	2.78	2.61
$E_1+\Delta_1$ (eV)	3.26	3.16	3.14	3.01	2.84
E_0' (eV)	4.5	4.4	4.4	4.3	
E_2 (eV)	4.95	4.85	4.80	4.70	4.60
A ($eV^{1.5}$)	4.3	3.6	3.6	3.0	2.5
B_1	4.0	4.0	4.0	4.0	4.0
B_{01}^*	12.36	12.30	12.24	12.18	12.06
B_2	2.0	2.0	2.0	2.0	2.0
B_{02}^*	6.19	6.17	6.14	6.12	6.06
B_{1x}^1 (eV)	1.1	1.1	1.1	1.1	1.1
B_{2x}^1 (eV)	0.55	0.55	0.55	0.55	0.55
Γ $[E_1/(E_1+\Delta_1)]$ (eV)	0.08	0.10	0.12	0.14	0.18
$C(E_0')$	0.922	0.736	0.640	0.239	
$\gamma(E_0')$	0.077	0.096	0.095	0.079	
$C(E_2)$	1.057	1.567	1.773	2.629	3.864
$\gamma(E_2)$	0.059	0.092	0.105	0.159	0.221
$\epsilon_{1\infty}$	1.4	1.0	1.2	1.2	0.7

present between the electrons and the holes. There may be only two analytical equations which enable us to treat the excitonic effects at the $E_1/(E_1+\Delta_1)$ spectral region: (1) the effective-mass (EM) approximation,[14,15] and (2) the Koster-Slater (KS) method.[16,17]

In the case of the 3D M_1 CP's (i.e., saddle-point excitons or hyperbolic excitons), the EM equation is much more difficult to solve. However, in the limit $m_L^{-1}\approx 0$ the equation gives a series of the 2D Wannier-type exciton (discrete exciton),[15]

$$E_{x1}^n(E_{x\Delta}^n)=-R_y^{2D}/(n-\tfrac{1}{2})^2 , \tag{10a}$$

$$|\phi_n^{2D}(0)|^2=\frac{16V_0}{\pi(a_B^{2D})^3(2n-1)^3} , \tag{10b}$$

where E_{x1}^n ($E_{x\Delta}^n$) is the exciton energy, $|\phi_n^{2D}(0)|$ the envelope function of the nth exciton, R_y^{2D} the exciton Rydberg energy, V_0 the volume of the unit cell, and a_B^{2D} the exciton Bohr radius. The contribution of the 2D-exciton transitions to $\epsilon(\omega)$ can now be written with Lorentzian line shape as

$$\epsilon(\omega)=\sum_{n=1}^{\infty}[B_{1x}^n(E_1+E_{x1}^n-\hbar\omega-i\Gamma)^{-1} +B_{2x}^n(E_1+\Delta_1+E_{x\Delta}^n-\hbar\omega-i\Gamma)^{-1}] , \tag{11}$$

where B_{1x}^n and B_{2x}^n are the exciton-strength parameters [proportional to $|\phi_n^{2D}(0)|^2$] at the E_1 and $E_1+\Delta_1$ CP's, respectively, and E_{x1}^n and $E_{x\Delta}^n$ are the corresponding exciton energies [see Eq. (10a)]. The 2D EM approximation also gives the continuum part of the excitonic states.[15] However, one can consider that the contribution of this part is similar to that of the one-electron approximation [i.e., Eqs. (1), (4), or (6)]. We thus neglect the continuum-exciton contribution to $\epsilon(\omega)$ in the present analysis.

In the KS method the electron-hole interaction (Coulomb potential) is evaluated in the tight-binding approximation and its attraction is approximated by an on-site contact interaction. An approximate expression of $\epsilon(\omega)$ based on this model is written as (Refs. 16 and 17)

$$\epsilon(\omega)-1=\frac{\tilde{\epsilon}(\omega)-1}{1-g[\tilde{\epsilon}(\omega)-1]} , \quad g>0 \tag{12}$$

where $\tilde{\epsilon}$ is the one-electron dielectric function and the parameter g is proportional to the depth of the assumed square-well potential. This expression was successfully used to show the presence of the excitonic effects in the E_1 structure of low-temperature electroreflectance data of Ge.[16]

In Fig. 2 we show calculated line shapes of the E_1 gap

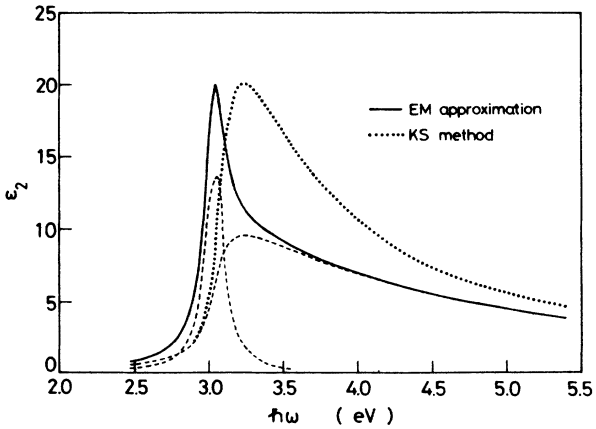

FIG. 2. Line shape of the E_1 gap contribution to ϵ_2 of GaAs (at 22 K). The solid line corresponds to a sum of the discrete exciton [Eq. (11); dashed line] and the one-electron terms [Eq. (6); dashed line]. The dotted line is the result of Eq. (12) with $g=0.065$.

contribution to ϵ_2 of GaAs (at 22 K). The solid line corresponds to a sum of the discrete exciton [Eq. (11); dashed line] and the one-electron terms [Eq. (6); dashed line]. Here in Eq. (11) we considered only the $n=1$ ground-state exciton, since the strengths of the $n \geq 2$ excited states are extremely weaker than that of the $n=1$ state [see Eq. (10b)]. The dotted line is the result of Eq. (12) with $g=0.065$. A difficulty arises in obtaining the one-electron dielectric function $\tilde{\epsilon}(\omega)$ to be inserted into Eq. (12), since this function is not directly measurable. We therefore assumed the dielectric function of Eq. (6) to be $\tilde{\epsilon}(\omega)$. The numerical values used are listed in Table I.

As we will see later, optical spectra in the $E_1/(E_1+\Delta_1)$ structure region of GaAs become sharp when the temperature is lowered. Such spectral change cannot be explained within the framework of the one-electron approximation with lifetime-broadening corrections. This fact is clearly suggestive of the contribution of excitonic effects to the $E_1/(E_1+\Delta_1)$ transitions. As seen in Fig. 2, not only the EM approximation (solid line) but also the KS method (dotted line) dramatically modifies and sharpens the $E_1/(E_1+\Delta_1)$ CP structure. However, the degree of sharpness is larger for the EM approximation than for the KS method. We found a better fit with the experiment using the EM approximation [i.e., taking into account the discrete exciton term of Eq. (11)].

B. E_2 (E_0') transitions

The more pronounced structure found in GaAs in the region higher in energy than E_1 is labeled E_2. The nature of the E_2 transitions is more complicated, since it does not correspond to a single, well defined CP. Because of this, we shall characterize the E_2 structure as that of a damped harmonic oscillator (DHO):

$$\epsilon_2(\omega)=C\chi_2\gamma/[(1-\chi_2^2)^2+\chi_2^2\gamma^2] , \tag{13}$$

$$\epsilon_1(\omega)=C(1-\chi_2^2)/[(1-\chi_2^2)^2+\chi_2^2\gamma^2] , \tag{14}$$

with

$$\chi_2=\hbar\omega/E_2 , \tag{15}$$

where C is the strength parameter and γ is the broadening energy divided by E_2 (i.e., $\gamma=\Gamma/E_2$, where Γ is in eV).

The E_2 transition region in GaAs evidences a multiplicity of the CP structure.[4,21,22] High-resolution electroreflectance measurements for GaAs at 4.2 K,[21] in fact, revealed various interband CP's in this transition region: E_0' ($\Gamma_8^v \rightarrow \Gamma_7^c$), $E_0'+\Delta_0'$ ($\Gamma_8^v \rightarrow \Gamma_8^c$), and $E_0'+\Delta_0'+\Delta_0$ ($\Gamma_7^v \rightarrow \Gamma_8^c$) at the Γ point, $E_0'(\Delta)$ and $E_0'+\Delta_0'$ (Δ) along the $\langle 100 \rangle$ directions (Δ) of the BZ, E_2 ($X_7^v \rightarrow X_6^c$, $X_6^v \rightarrow X_6^c$, $X_7^v \rightarrow X_7^c$, and $X_8^v \rightarrow X_7^c$) at the X point, and E_2 with Σ symmetry in an extended region of the BZ. Second-derivative spectroscopic ellipsometry at 22 K (Ref. 4) also revealed five structures (three E_0' CP's and two E_2 CP's) in the E_2 transition region. However, at higher temperatures only a few structures could be distinguished in this spectral region.

If the E_0' transitions occur at Γ (Δ), then the CP should be of 3D M_0 (3D M_1) type. These transitions dominate the E_2 transitions in the case of InP.[23] However, we found that neither a 3D M_0 nor the 3D M_1 model represents the line shapes of $\epsilon(\omega)$ in the E_0' region. The best fit was found with the DHO, as in the case of the E_2 CP's for some III-V binaries (such as GaP, GaSb, and InAs) (Ref. 5), $Al_xGa_{1-x}As$ (Ref. 6), $In_{1-x}Ga_xAs_yP_{1-y}$ (Ref. 8), Si (Ref. 7), Ge (Ref. 7), and α-Sn (Ref. 9). Therefore, we shall treat both the E_2 and E_0' transitions in GaAs as the DHO's [Eqs. (13) and (14)].

The DHO is thought to be a different representation of a 2D M_1 CP.[6] The contribution to ϵ_2 of the 2D M_1 CP is

$$\epsilon_2(\omega)=\pi\chi_2^{-2}(C_1\ln|1-x_2|-C_2) , \tag{16}$$

where C's are the strength parameters. Equation (16) exhibits a divergence at $\chi_2=1.0$ ($\hbar\omega=E_2$), and its spectrum resembles that of the DHO when we introduce the broadening energy Γ in the expression. The broadening effect ensure that the smaller the Γ value, the narrower the spectrum.

Many-particle effects on CP's in the interband continuum of semiconductors have been treated with their detailed electronic-energy band structures.[19,20] Results have shown that the absorption at the E_2 CP is markedly weakened, with no drastic change in its shape, by introducing the excitonic interaction. Unfortunately, however, no analytical line shape suitable to fit the excitonic-effect-influenced E_2 line shape has been reported to date. We find later that the DHO model is a good representation for the E_2 CP both with and without the presence of the excitonic interaction. The strength parameter C in Eqs. (13) and (14) (DHO) may, in principle, be independent of the temperature. Thus, the change in C values can account for the excitonic interaction strength at the E_2 CP (see Sec. III B). [The γ (Γ) in Eqs. (13) and (14) accounts for the electron-phonon interaction strength, i.e., broadening interaction.]

C. E_0 and $E_0+\Delta_0$ transitions

The E_0 and $E_0+\Delta_0$ transitions in the diamond- and zinc-blende-type semiconductors occur in the center of the BZ. These transitions are of the 3D M_0 CP's. Assuming the bands are parabolic, and using the KK relations, we obtain the contribution of these band gaps to $\epsilon_2(\omega)$ and $\epsilon_1(\omega)$ (Refs. 5–9):

$$\epsilon_2(\omega)=[A/(\hbar\omega)^2][(\hbar\omega-E_0)^{0.5}H(\chi_0-1) + \tfrac{1}{2}(\hbar\omega-E_0-\Delta_0)^{0.5}H(\chi_{s.o.}-1)] , \tag{17}$$

$$\epsilon_1(\omega)=AE_0^{-1.5}\{f(\chi_0)+\tfrac{1}{2}[E_0/(E_0+\Delta_0)]^{1.5}f(\chi_{s.o.})\} , \tag{18}$$

with

$$A=\tfrac{4}{3}(\tfrac{3}{2}m^*)^{1.5}P^2 , \tag{19}$$

$$f(\chi_0)=\chi_0^{-2}[2-(1+\chi_0)^{0.5}-(1-\chi_0)^{0.5}H(1-\chi_0)] , \tag{20a}$$

$$f(\chi_{s.o.})=\chi_{s.o.}^{-2}[2-(1+\chi_{s.o.})^{0.5} -(1-\chi_{s.o.})^{0.5}H(1-\chi_{s.o.})] , \quad (20b)$$

$$\chi_0=\hbar\omega/E_0 , \quad (21)$$

$$\chi_{s.o.}=\hbar\omega/(E_0+\Delta_0) , \quad (22)$$

where m^* is the combined density-of-states mass, P^2 is the squared momentum matrix element, and the H's are functions defined by Eq. (5).

Let us now consider the contribution of the exciton transitions to $\epsilon(\omega)$ at the lowest-direct band edge. It is well known[12] that the discrete lines and continuum excitons in the neighborhood of the lowest-direct band edge (3D M_0 CP) drastically change the optical spectrum. The discrete series of exciton lines at the E_0 gap can be simply given with Lorentzian line shape by

$$\epsilon(\omega)=\sum_{n=1}^{\infty} A_{0x}^{n}(E_0+E_{x0}^{n}-\hbar\omega-i\Gamma)^{-1} , \quad (23)$$

where A_{0x}^{n} is the exciton-strength parameter, and E_{x0}^{n} is the exciton energy written as

$$E_{x0}^{n}=-R_y^{3D}/n^2 . \quad (24)$$

In Eq. (24), R_y^{3D} is the 3D exciton Rydberg energy. Like the 2D Wannier excitons presented in Sec. II A, the 3D Wannier-type exciton parameter A_{0x}^{n} in Eq. (23) is proportional to the envelope function $[|\phi_n^{3D}(0)|^2]$ of the nth exciton:

$$|\phi_n^{3D}(0)|^2=\frac{V_0}{\pi(a_B^{3D})^3 n^3} , \quad (25)$$

where a_B^{3D} is the 3D exciton Bohr radius.

The continuum-exciton transitions at the 3D M_0 CP behave like the noninteracting electron-hole–pair characteristics. The contribution of these transitions to $\epsilon(\omega)$ can therefore be considered with expressions similar to Eqs. (17) and (18).

In Fig. 3 we show the calculated spectral dependence of $\epsilon_2(\omega)$ in the neighborhood of the E_0 edge of GaAs. The solid circles are the experimental data taken from Ref. 24. The dashed line is obtained without taking into account the excitonic effects, and the solid line is the result taking into account the discrete exciton series [i.e., Eq. (23)]. The band-gap energies and the noninteracting strength parameters used are as follows: $E_0=1.5227$ eV ($E_0=1.423$ eV) and $A=4.3$ eV$^{1.5}$ ($A=3.45$ eV$^{1.5}$) at 21 K (294 K). The exciton parameters used are $A_{0x}^{1}=2.35\times10^{-3}$ eV ($A_{0x}^{n}=A_{0x}^{1}/n^3$ eV) and $R_y^{3D}=4.7$ meV (Ref. 25). The exciton-broadening energies (Γ) determined from these fits are 5.0 and 25 meV at 21 and 294 K, respectively. It is evident from the figure that the inclusion of the discrete-exciton contribution (solid lines) is a great improvement over the noninteracting electron-hole–pair model (dashed lines). However, the discrete-exciton states are present only in the limited region close to the E_0 edge and their strength is considerably weaker than that of the ensuring E_1, $E_1+\Delta_1$, and E_2 (E_0') (see Fig. 4). The contribution of these states is thus not so important, and can be neglected in the following analyses.

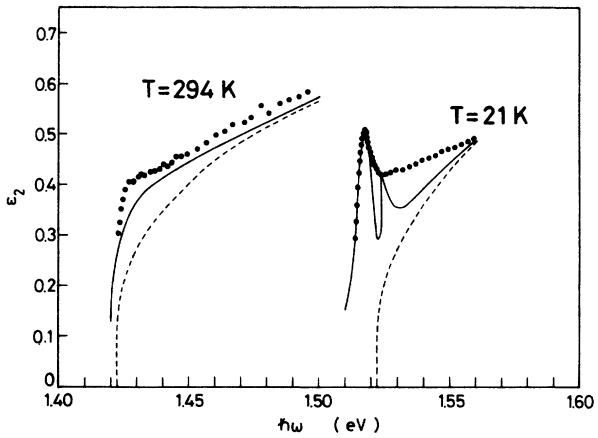

FIG. 3. Calculated spectral dependence of $\epsilon_2(\omega)$ in the neighborhood of the E_0 edge of GaAs. The solid circles are the experimental data taken from Ref. 24. The dashed line is obtained without taking into account the excitonic effects at the E_0 edge, and the solid line is the result taking into account the discrete exciton series [i.e., Eq. (23)].

III. ANALYSIS AND DISCUSSION

A. Comparison of our model to experimental spectra

The fit with our model to the experimental ϵ_2 of GaAs at 22 K is shown in Fig. 4. The solid line is obtained from the sum of Eqs. (6), (11), (13), and (17). The dashed

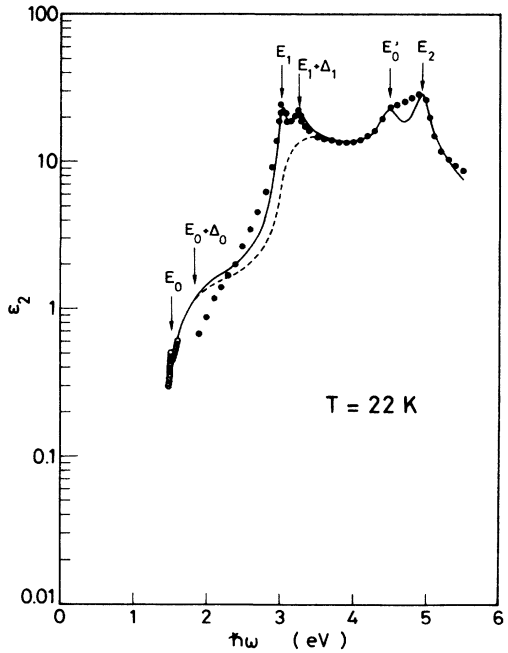

FIG. 4. ϵ_2 spectrum of GaAs at 22 K. The experimental data are taken from Refs. 24 ($T=21$ K; open circles) and 4 (solid circles). The solid line is obtained from the sum of Eqs. (6) ($\Gamma=0.08$ eV), (11) ($\Gamma=0.08$ eV), (13), and (17). The dashed line is the result of the sum of Eqs. (6), (13), and (17) [i.e., without taking into account the saddle-point exciton contribution, Eq. (11)].

line is the result of the sum of Eqs. (6), (13), and (17) [i.e., without taking into account the saddle-point exciton contribution, Eq. (11)]. The numerical parameters of the fit are listed in Table I. We have made the assumption $R_y^{2D}=0$, since the detailed value is not yet well known. Since the 2D ground-state exciton term ($n=1$) in Eq. (11) contains 95% of the total oscillator strength, we neglected the excited-state terms ($n\geq 2$) in our calculation. The experimental data are taken from Refs. 24 (open circles) and 4 (solid circles).

There is an accumulation of interband CP's in the energy range 4.5–5.5 eV. This accumulation consists of the E_2 and E_0' multiplets.[21,22] We considered for simplicity only two DHO's [E_0' ($=4.5$ eV) and E_2 ($=4.95$ eV)] in this spectral region. As discussed in Sec. II A, we are able to fit the $E_1/(E_1+\Delta_1)$ CP structure with either the 3D M_1 [Eq. (1)] or the 2D M_0 model [Eq. (4)]. Both models explained the peculiar structure of the $E_1/(E_1+\Delta_1)$ CP well, but, unfortunately, they required other dispersion mechanism, namely the indirect-band-gap–transition mechanism, in the region below the $E_1/(E_1+\Delta_1)$ CP's.[5,6] Although the mechanism should exist in actual optical transitions, the strength parameter determined by this fitting is seemed to be considerably large. Our new expression of Eq. (6), on the other hand, can account reasonably well for such a compulsory contribution as a low-energy-tail component of the $E_1/(E_1+\Delta_1)$ gap contribution when we properly take account of the broadening energy Γ ($=0.08$ eV) in the expression. It is clear from Fig. 4 that the sharp peaks appearing at the $E_1/(E_1+\Delta_1)$ edge region cannot be explained only by this one-electron approximation (dashed line). The saddle-point exciton model of Eq. (11) can successfully improve the fit in this energy region. The best-fitted exciton parameters are $B_{1x}^{1}=1.1$ eV, $B_{2x}^{1}=0.55$ eV, and $\Gamma=0.08$ eV. Excellent agreement is then achieved between our calculation and the experimental values over the entire range of photon energies.

A comparison of our calculated $\epsilon_1(\omega)$ to the experimental data of GaAs at 22 K is shown in Fig. 5. The calculated curve is obtained from the sum of Eqs. (7) ($\Gamma=0.08$ eV), (11) ($\Gamma=0.08$ eV), (14), and (18). The solid circles are the experimental data taken from Ref. 4. The data of $\epsilon_1(\omega)$ in the transparent region are usually somewhat larger than those of our model. In order to improve a fit, therefore, we considered an additional term, $\epsilon_{1\infty}$, to $\epsilon_1(\omega)$ (see Table I). This term is assumed to be nondispersive (i.e., constant) and may arise from other higher-lying, interband transitions (E_1', $E_1'+\Delta_1'$, $E_2+\Delta_2$, etc.).

When we insert $\Gamma=0$ eV into Eq. (7) or (11), their calculated spectra exhibit a divergence at the E_1 and $E_1+\Delta_1$ edges. As shown in Fig. 5, a properly chosen value of Γ can decrease the strength of the $E_1/(E_1+\Delta_1)$ peak and leads to a fact which is coincident with the experimental verification. [It is also noteworthy that the value of Γ ($=0.08$ eV) determined from $\epsilon_1(\omega)$ is in quite good agreement with that obtained from $\epsilon_2(\omega)$ (Fig. 4).] We also recognize in Fig. 5 a considerable deviation of our model from the experimental data in the energy region at ~ 4.5 eV ($E_0'-E_2$), i.e., the calculated ϵ_1 spectrum shows a distinct structure in the ~ 4.5-eV region. This seems nonessential: if one consider (an) additional oscillator(s) [DHO('s)] in this energy region, the discrepancy may be lost or a better fit may be achieved, not only for $\epsilon_1(\omega)$, but also for $\epsilon_2(\omega)$ (see Fig. 4), although we have not actually performed such a fit.

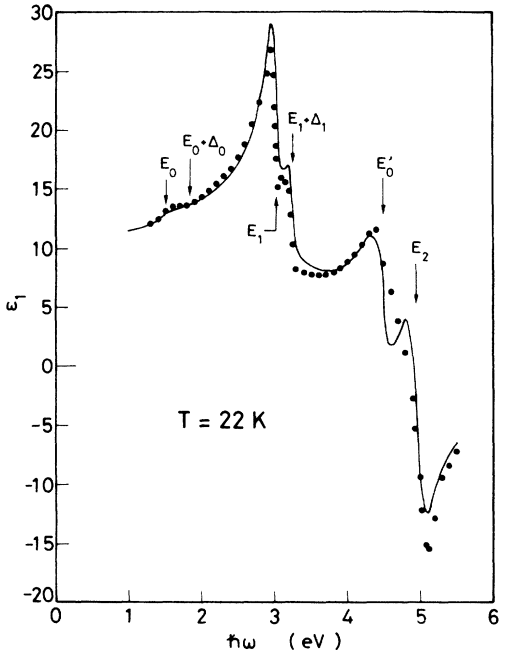

FIG. 5. ϵ_1 spectrum of GaAs at 22 K. The solid circles are the experimental data taken from Ref. 4. The solid line is obtained from the sum of Eqs. (7) ($\Gamma=0.08$ eV), (11) ($\Gamma=0.08$ eV), (14), (18), and $\epsilon_{1\infty}$ ($=1.4$).

In Fig. 6 we show the fit with our model to the experimental ϵ_2 of GaAs at 300 K. The solid line is obtained from the sum of Eqs. (6) ($\Gamma=0.12$ eV), (11) ($\Gamma=0.12$ eV), (13), and (17). The dashed line is the result of the sum of Eqs. (6), (13), and (17) [i.e., without taking into account the saddle-point exciton contribution, Eq. (11)]. The experimental data are taken from Refs. 24 (294 K; open circles) and 3 (solid circles). It is clear that the saddle-point exciton model of Eq. (11) (solid line) successfully improves the fit in the $E_1/(E_1+\Delta_1)$ structure region. The Γ value at 300 K is 0.12 eV, which is larger than that determined at 22 K ($\Gamma=0.08$ eV).

The fit with our model to the experimental ϵ_1 of GaAs at 300 K is shown in Fig. 7. The theoretical curve is obtained from the sum of Eqs. (7), (11), (14), (18), and $\epsilon_{1\infty}$ ($=1.2$). The experimental data are taken from Refs. 26 (open circles) and 3 (solid circles). The Γ value used in Eqs. (7) and (11) is 0.12 eV, which is the same as that determined from $\epsilon_2(\omega)$ (Fig. 6). Excellent agreement can be achieved between our model and the experimental data over a wide range of photon energies.

Figure 8 shows the fit with our model to the experimental $\epsilon_2(\omega)$ spectrum of GaAs at 504 K. The solid line is obtained from the sum of Eqs. (6) ($\Gamma=0.14$ eV), (11) ($\Gamma=0.14$ eV), (13), and (17). The dashed line is the result of the sum of Eqs. (6), (13), and (17) [i.e., without taking

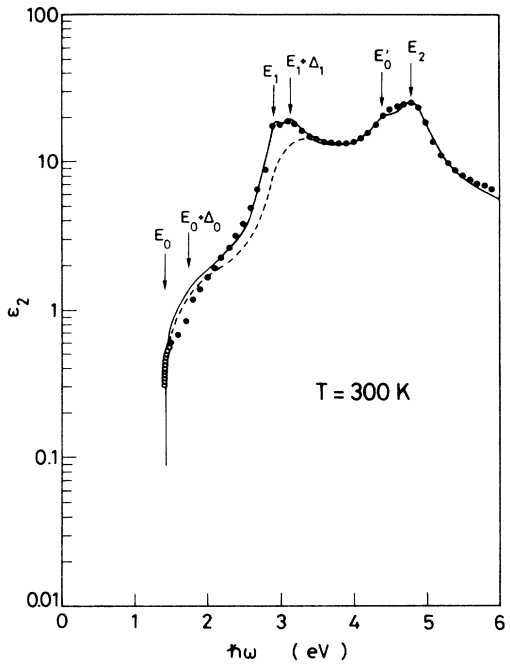

FIG. 6. ϵ_2 spectrum of GaAs at 300 K. The experimental data are taken from Refs. 24 ($T=294$ K; open circles) and 3 (solid circles). The solid line is obtained from the sum of Eqs. (6) ($\Gamma=0.12$ eV), (11) ($\Gamma=0.12$ eV), (13), and (17). The dashed line is the result of the sum of Eqs. (6), (13), and (17) [i.e., without taking into account the saddle-point exciton contribution, Eq. (11)].

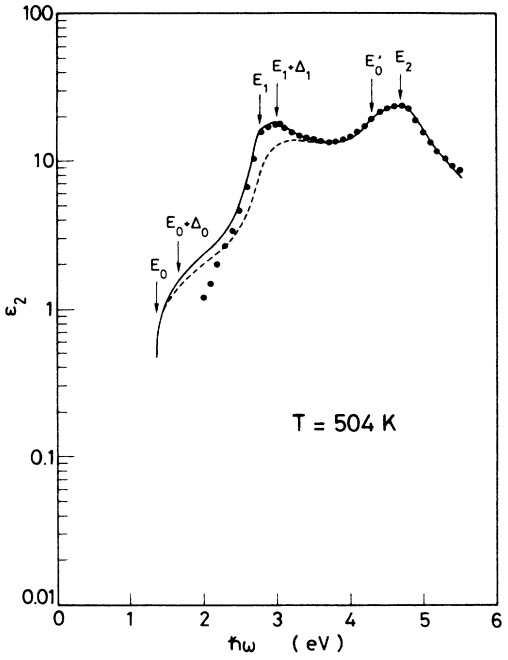

FIG. 8. ϵ_2 spectrum of GaAs at 504 K. The solid circles are the experimental data taken from Ref. 4. The solid line is obtained from the sum of Eqs. (6) ($\Gamma=0.14$ eV), (11) ($\Gamma=0.14$ eV), (13), and (17). The dashed line is the result of the sum of Eqs. (6), (13), and (17) [i.e., without taking into account the saddle-point exciton contribution, Eq. (11)].

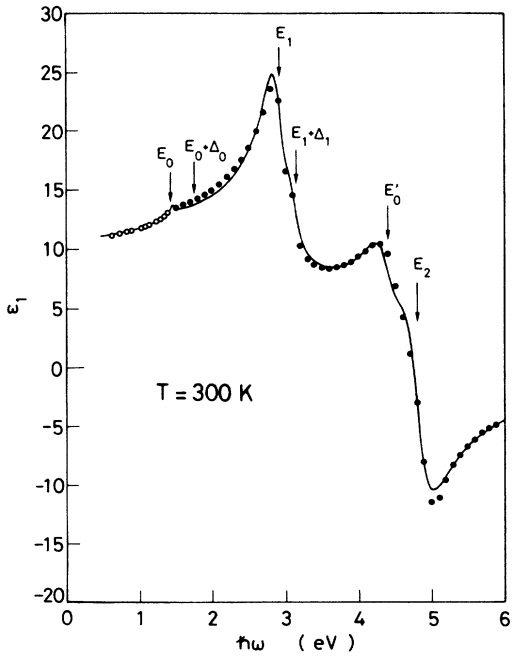

FIG. 7. ϵ_1 spectrum of GaAs at 300 K. The experimental data are taken from Refs. 26 (open circles) and 3 (solid circles). The solid line is obtained from the sum of Eqs. (7) ($\Gamma=0.12$ eV), (11) ($\Gamma=0.12$ eV), (14), (18), and $\epsilon_{1\infty}$ ($=1.2$).

into account the saddle-point exciton contribution, Eq. (11)]. The solid circles are the experimental data taken from Ref. 4.

As seen in the figure, the calculated $\epsilon_2(\omega)$ spectrum at 504 K becomes quite satisfactory when the saddle-point exciton contribution is taken into consideration (solid line). This is just as in the cases at 22 (Fig. 4) and 300 K (Fig. 6). However, the exciton-induced sharp peaks disappeared at 504 K in both the calculated and experimental spectra. This is a consequence of a relatively strong exciton-phonon interaction at this temperature. The best-fitted Γ value at 504 K is 0.14 eV, which is considerably larger than that determined at 22 K ($\Gamma=0.08$ eV). We can also see that the E_2 (E_0') structure at 504 K becomes much broader and the spectral region is successfully explained only by two DHO's [E_0' ($=4.3$ eV) and E_2 ($=4.70$ eV); Eq. (13)], in contrast to that at 22 K, where, as mentioned before, a few more oscillators should be required in the region at 22 K for achieving complete agreement with the experimental data. Relatively poor agreement of the fit can be seen in the neighborhood of the $E_0/(E_0+\Delta_0)$ structure region. Because of the poor accuracy of the experiment at this low-ϵ_2 region,[4] we do not discuss this problem in detail.

The fit with our model to the experimental ϵ_1 of GaAs at 504 K is shown in Fig. 9. The theoretical curve is obtained from the sum of Eqs. (7), (11), (14), (18), and $\epsilon_{1\infty}$ ($=1.2$). The experimental data are taken from Ref. 4

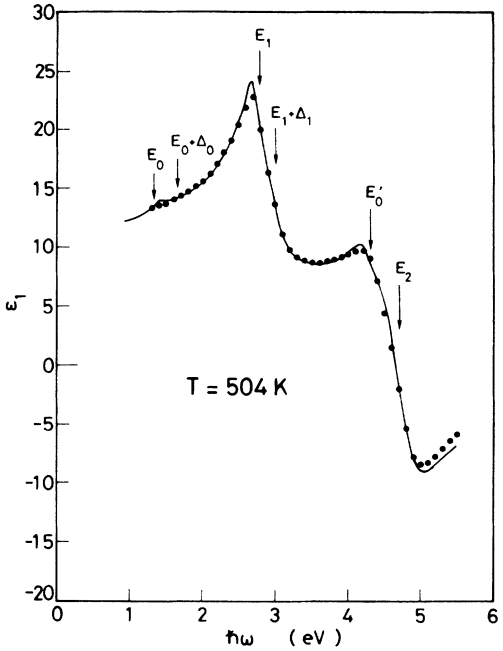

FIG. 9. ϵ_1 spectrum of GaAs at 504 K. The solid circles are the experimental data taken from Ref. 4. The solid line is obtained from the sum of Eqs. (7) ($\Gamma=0.14$ eV), (11) ($\Gamma=0.14$ eV), (14), (18), and $\epsilon_{1\infty}$ ($=1.2$).

(solid circles). The Γ value used in Eqs. (7) and (11) is 0.14 eV, which is the same as that determined from $\epsilon_2(\omega)$ (Fig. 8). As can be seen in the figure, this Γ value interprets the experimental $E_1/(E_1+\Delta_1)$ peak value at ~ 2.7 eV well. Excellent agreement can then be achieved between our model and the experimental data over a wide range of photon energies.

An individual contribution to ϵ_2 of the $E_1/(E_1+\Delta_1)$, E_2 (E_0'), and $E_0/(E_0+\Delta_0)$ gaps for GaAs at 22 and 504 K is shown in Figs. 10 and 11, respectively. They are ob-

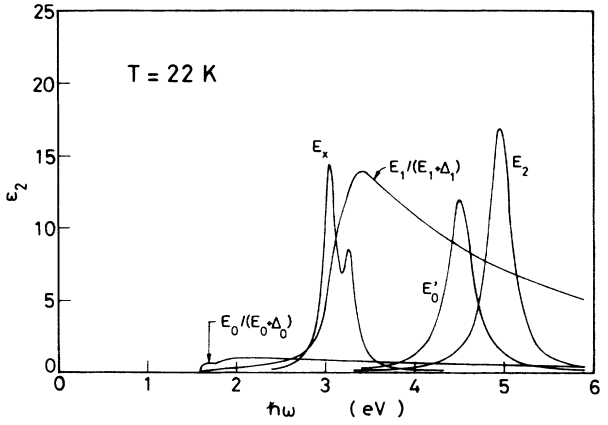

FIG. 10. An individual contribution to ϵ_2 of the $E_1/(E_1+\Delta_1)$, E_2 (E_0'), and $E_0/(E_0+\Delta_0)$ gaps for GaAs at 22 K. They are obtained from Eqs. (6) and (11) ($\Gamma=0.08$ eV) for the $E_1/(E_1+\Delta_1)$ gap contribution, from Eq. (13) for the E_2 (E_0') gap contribution, and from Eq. (17) for the $E_0/(E_0+\Delta_0)$ gap contribution.

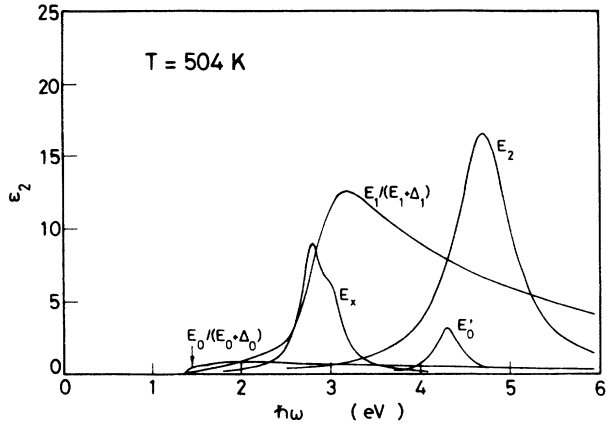

FIG. 11. An individual contribution to ϵ_2 of the $E_1/(E_1+\Delta_1)$, E_2 (E_0'), and $E_0/(E_0+\Delta_0)$ gaps for GaAs at 504 K. They are obtained from Eqs. (6) and (11) ($\Gamma=0.14$ eV) for the $E_1/(E_1+\Delta_1)$ gap contribution, from Eq. (13) for the E_1 (E_0') gap contribution, and from Eq. (17) for the $E_0/(E_0+\Delta_0)$ gap contribution.

tained from Eqs. (6) and (11) ($\Gamma=0.08$ eV at 22 K, $\Gamma=0.14$ eV at 504 K) for the $E_1/(E_1+\Delta_1)$ gap contribution, from Eq. (13) for the E_2 (E_0') gap contribution, and from Eq. (17) for the $E_0/(E_0+\Delta_0)$ gap contribution.

The E_1 and $E_1+\Delta_1$ gaps are of the 3D M_1 (or 2D M_0) type. Hence, the line shape of the corresponding ϵ_2 spectrum should be characterized by a steep low-energy side and a broader high-energy side. The calculated exciton contribution at the $E_1/(E_1+\Delta_1)$ edges at low temperature (22 K) gives sharp ϵ_2 peaks in this spectral region, in good agreement with the experimental data. At higher temperature (504 K), these peaks are strongly influenced by the exciton-phonon interaction and, as a result, they become considerably broader.

The E_2 structure can be characterized by the DHO well [Eq. (13)]. This model of $\epsilon_2(\omega)$ gives a Lorentzian-type line shape, and ensures that the higher the temperature, the broader the spectrum. The broadening parameters obtained are $\gamma=0.059$ ($\Gamma=\gamma E_2=0.29$ eV) at 22 K and $\gamma=0.159$ ($\Gamma=0.75$ eV) at 504 K. The corresponding $\epsilon_1(\omega)$ spectra [Eq. (14)] interpreted the strong negative peaks which appeared experimentally in this structure region (see Figs. 5, 7, and 9).

The transitions at the 3D M_0 edges $[E_0/(E_0+\Delta_0)]$ yield a continuous absorption obeying the well-known $\frac{1}{2}$-power law [i.e., $\propto(\hbar\omega-E_0)^{0.5}$]. These transitions strongly contribute to the dispersion of $\epsilon_1(\omega)$, but not to its absolute value. The 3D M_0 excitonic transitions are very weak, so the structure in $\epsilon_2(\omega)$ is only visible at the E_0 edge at low temperatures (see Fig. 3).

B. Strength and broadening parameters as a function of temperature

The strength of the $E_1/(E_1+\Delta_1)$ transitions is represented by B_1 (E_1) and B_2 ($E_1+\Delta_1$) [see Eqs. (6) and (7)]. In Fig. 12 we show the variation of B_1, B_2, and Γ as

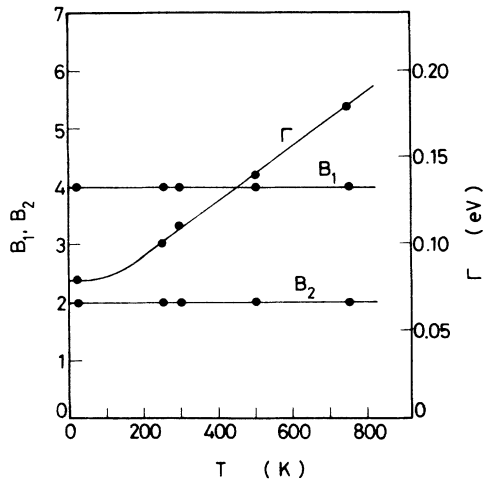

FIG. 12. The strength parameters B_1 and B_2 and broadening parameter Γ [$E_1/(E_1+\Delta_1)$ transitions] as a function of temperature T for GaAs.

a function of temperature ($T=22-754$ K) for GaAs. The strength of the $E_1/(E_1+\Delta_1)$ transitions of zinc-blende-type materials can be theoretically estimated with the simple expressions[4,27–33]

$$B_1=44\frac{E_1+(\Delta_1/3)}{a_0E_1^2}\ , \tag{26a}$$

$$B_2=44\frac{E_1+(2\Delta_1/3)}{a_0(E_1+\Delta_1)^2}\ , \tag{26b}$$

where A_0 is the lattice constant in Å and E_1 and Δ_1 are in eV. The calculated results suggest that both B_1 and B_2 are only slowly increasing functions of temperature from 2.6 (22 K) to 3.1 (754 K) for B_1 and from 2.3 (22 K) to 2.7 (754 K) for B_2, while the experimentally determined B_1 and B_2 do not depend on the temperature within our fitting accuracy. The sum of the calculated B_1 and B_2 is between 4.9 (22 K) and 5.8 (754 K), while the sum of the experimental B_1 and B_2 is 6.0 over the whole temperature range (22–754 K). The agreement seems to be good in view of the crudeness of the theory used. The ratio of the calculated B_1/B_2 at 22 K is 1.1, while the experiment gives $B_1/B_2=2.0$. Some calculations[34,35] showed that a correction for terms linear in $\mathbf{k}$ for $\mathbf{k}$ perpendicular to $\langle 111\rangle$ increases the strength of the E_1 transitions relative to the $E_1+\Delta_1$. This tendency is in qualitative agreement with the present result.

The experimental 2D-exciton strengths are $B^{\rm I}_{1x}=1.1$ eV and $B^{\rm I}_{2x}=0.55$ eV over the whole temperature range. These values are considerably larger than those of the 3D M_0 excitons ($A^{\rm I}_{0x}=2.35\times10^{-3}$ eV). The corresponding ratio $B^{\rm I}_{1x}/B^{\rm I}_{2x}$ is 2.0, in exact coincidence with the experimental ratio B_1/B_2 of the one-electron transitions. (The result seems to be reasonable as the first principle, although it is difficult to attribute a physical significance to this result.)

If we label the electron (exciton) –LO-phonon coupling as the main broadening mechanism, its parameter value can be expressed by a sum of two different contributions: $\Gamma(T)=\Gamma_0+\Gamma_\Xi(T)$, where Γ_0 is independent of the temperature T, arising mainly from crystalline imperfections, and $\Gamma_\Xi(T)$ is a contribution through emission and absorption of LO phonons of average frequency Ξ, proportional to $[\exp(\Xi/T)-1]^{-1}$. This expression ensures a relatively constant Γ value from low T up to, in many cases, $T\approx50-200$ K, at which point a component Γ_Ξ becomes discernible, and then increases nearly proportionally to T for high T. As seen in Fig. 12, this behavior of $\Gamma(T)$ is the same as that obtained for the $E_1/(E_1+\Delta_1)$ transitions (one-electron and saddle-point excitonic transitions).

The strength of the E_2 transitions is represented by C [see Eqs. (13) and (14)]. The variation of C and γ as a function of temperature for GaAs is shown in Fig. 13.

As is clearly seen in Figs. 2 and 3, the 3D M_0 and saddle-point excitons profoundly modified the CP (Van Hove singularity) structures. However, we can find no clear change in the spectrum at the E_2 region due to the excitonic interaction. In a broad class of group-IV elemental and III-V and II-VI compounds, the calculated spectrum within the one-electron approximation yielded an E_1 peak with less strength than measured, but elicited an E_2 peak with more strength than the measured one. These discrepancies have prompted studies of excitonic effects on the optical spectra of these semiconductors,[15,19,20] and the inclusion of the excitonic effects has led to an improvement over the one-electron approximation in the sense that the E_1 peak becomes stronger and the E_2 peak weaker. These studies also indicated that if one takes into account the excitonic effects, the E_1 structure becomes relatively sharp, but the E_2 structure shows no rigorous change in its line shape.

The excitonic effects may dominantly take part in spectra at low temperatures. The experimental variation of C suggested that the lower the temperature, the smaller the C value. This temperature dependence is in reasonable

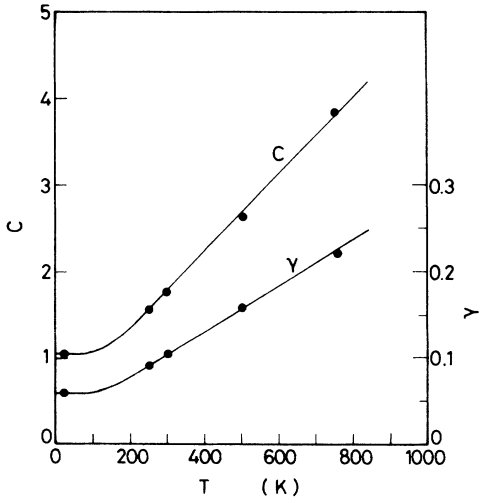

FIG. 13. The strength parameter C and broadening parameter γ (E_2 transitions) as a function of temperature T for GaAs.

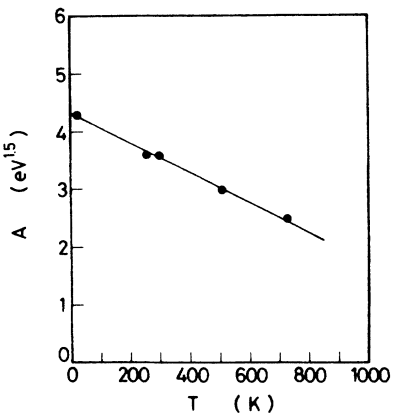

FIG. 14. The strength parameter A [$E_0/(E_0+\Delta_0)$ transitions] as a function of temperature T for GaAs.

agreement with that expected from the theoretical consideration, i.e., the smaller C value at lower T may be due to the excitonic interaction at the E_2 edge. There is also only one theoretical report[20] that suggests a formation of E_2-related excitonic bound states below the E_2 edge in Si and Ge. Our fit, however, required no bound states in the region near the E_2 edge even at low temperatures. The γ value obtained is almost constant up to $T\approx 100$ K, and increases nearly proportionally to T. This temperature dependence of γ is the same as that observed for the $E_1/(E_1+\Delta_1)$ transitions (Fig. 10). The sharpening of the E_2 structure with reduced T (see Figs. 10 and 11) may thus be only due to the reduction of the electron-phonon interaction (but not due to any intrinsic excitonic effect).

The strength of the $E_0/(E_0+\Delta_0)$ transitions is represented by A [see Eqs. (17) and (18)]. The numerical values of A as a function of temperature for GaAs are shown in Fig. 14. The parameter A may, in principle, be independent of the temperature. The plots, however, suggest that A decreases almost linearly with increasing temperature. As mentioned in Sec. II C, the continuum-exciton transitions at the 3D M_0 CP behave like the noninteracting one-electron characteristics [i.e., Eqs. (17) and (18)]. However, we did not take into account these exciton states in our analyses. We can therefore consider that relatively large values of A at lower temperatures are the result of the continuum-exciton modification of $\epsilon(\omega)$ at the 3D M_0 CP. Unfortunately, however, it is difficult to proceed with detailed discussion on this problem because of the poor accuracy of the experimental ϵ for small ϵ (and also the poor fits of our analyses) in this spectral region.

IV. CONCLUSIONS

We have presented a calculation of the real (ϵ_1) and imaginary (ϵ_2) parts of the dielectric function of semiconductors at energies below and above the fundamental absorption edge. This model includes the E_0, $E_0+\Delta_0$, E_1, $E_1+\Delta_1$, and E_2 (E_0') transitions as the main dispersion mechanisms (the noninteracting electron-hole excitations). At low temperatures, optical spectra cannot be explained within the framework of this noninteracting approximation, since the excitonic effect may profoundly modify the critical-point (CP) singularity structure at low temperatures. Therefore, the model accounts for the excitonic effects at these CP's [the three-dimensional discrete excitons at the E_0 CP, the saddle-point (discrete) excitons at the E_1 and $E_1+\Delta_1$ CP's, and the continuum-state excitons at the E_2 CP]. A model analysis has shown that the inclusion of the excitonic effects in our noninteracting, one-electron model corrects the strength of the peaks in the correct direction with experimental information (i.e., the E_1 peak becomes stronger and the E_2 peak weaker). Detailed analyses are presented for GaAs in the temperature range between 22 and 754 K, and the results are in satisfactory agreement with the experimental data over the entire range of photon energies (0.0–6.0 eV). The temperature dependence of the strength and the broadening parameters at each CP are also given and discussed.

ACKNOWLEDGMENTS

This work was supported in part by the Gunma University Foundation for Science and Technology, Gunma, Japan.

[1] J. Friedel, G. Harbeke, F. Abelès, B. O. Seraphin, J. Tauc, V. Spicer, J. Ducuing, and C. Flytzanis, in *Optical Properties of Solids,* edited by F. Abelès (North-Holland, Amsterdam, 1976).
[2] H. C. Casey, Jr., and M. B. Panish, *Heterostructure Lasers* (Academic, New York, 1978), Pts. A and B.
[3] D. E. Aspnes and A. A. Studna, Phys. Rev. B **27**, 985 (1983).
[4] P. Lautenschlager, M. Garriga, S. Logothetidis, and M. Cardona, Phys. Rev. B **35**, 9174 (1987).
[5] S. Adachi, Phys. Rev. B **35**, 7454 (1987).
[6] S. Adachi, Phys. Rev. B **38**, 12 345 (1988).
[7] S. Adachi, Phys. Rev. B **38**, 12 966 (1988).
[8] S. Adachi, Phys. Rev. B **39**, 12 612 (1989).
[9] S. Adachi, J. Appl. Phys. **66**, 813 (1989).
[10] S. Adachi, J. Appl. Phys. **66**, 3224 (1989).
[11] S. Adachi, Jpn. J. Appl. Phys. **28**, 1536 (1989).
[12] R. J. Elliott, Phys. Rev. **108**, 1384 (1957).
[13] J. C. Phillips, Phys. Rev. **136**, A1705 (1964).
[14] E. O. Kane, Phys. Rev. **180**, 852 (1969).
[15] B. Velický and J. Sak, Phys. Status Solidi **16**, 147 (1966).
[16] J. E. Rowe and D. E. Aspnes, Phys. Rev. Lett. **25**, 162 (1970).
[17] R. M. Martin, J. A. Van Vechten, J. E. Rowe, and D. E. Aspnes, Phys. Rev. B **6**, 2500 (1972).
[18] M. Welkowsky and R. Braunstein, Phys. Rev. B **5**, 497 (1972).
[19] W. Hank and L. J. Sham, Phys. Rev. B **21**, 4656 (1980).
[20] M. del Castillo-Mussot and L. J. Sham, Phys. Rev. B **31**, 2092 (1985).
[21] D. E. Aspnes and A. A. Studna, Phys. Rev. B **7**, 4605 (1973).
[22] J. R. Chelikowsky and M. L. Cohen, Phys. Rev. B **14**, 556 (1976).

[23]S. M. Kelso, D. E. Aspnes, M. A. Pollack, and R. E. Nahory, Phys. Rev. B **26**, 6669 (1982).
[24]M. D. Sturge, Phys. Rev. **127**, 768 (1962).
[25]S. Adachi, J. Appl. Phys. **58**, R1 (1985).
[26]B. O. Seraphin and H. E. Bennett, in *Semiconductors and Semimetals*, edited by R. K. Willardson and A. C. Beer (Academic, New York, 1967), Vol. 3.
[27]L. Viña, C. Umbach, M. Cardona, and L. Vodopyanov, Phys. Rev. B **29**, 6752 (1984).
[28]L. Viña, S. Logothetidis, and M. Cardona, Phys. Rev. B **30**, 1979 (1984).
[29]S. Logothetidis, L. Viña, and M. Cardona, Phys. Rev. B **31**, 947 (1985).
[30]L. Viña, H. Höchst, and M. Cardona, Phys. Rev. B **31**, 958 (1985).
[31]S. Logothetidis, M. Cardona, P. Lautenschlager, and M. Garriga, Phys. Rev. B **34**, 2458 (1986).
[32]P. Lautenschlager, M. Garriga, and M. Cardona, Phys. Rev. B **36**, 4813 (1987).
[33]P. Lautenschlager, M. Garriga, L. Viña, and M. Cardona, Phys. Rev. B **36**, 4821 (1987).
[34]A. Daunois and D. E. Aspnes, Phys. Rev. B **18**, 1824 (1978).
[35]M. Cardona, Phys. Rev. B **15**, 5999 (1977).